

Empirical fundamental equation of state for phosgene based on molecular simulation data

Gábor Rutkai and Jadran Vrabec*

*Lehrstuhl für Thermodynamik und Energietechnik, Universität Paderborn, 33098
Paderborn, Germany*

E-mail: jadran.vrabec@upb.de

Phone: +49-5251/60-2421

Abstract

It is reported on an automatized empirical fundamental equation of state fitting approach that is based on molecular simulation data. In total 400 state points are sampled in the homogeneous fluid region for temperatures between 150 K and 700 K up to a pressure of 550 MPa and a density of $17.6 \text{ mol}\cdot\text{dm}^{-3}$. At each state point six thermodynamic properties are calculated. These properties are different partial derivatives of the Helmholtz energy divided by the temperature with respect to inverse temperature and density. The present equation of state itself is also explicit in terms of this thermodynamic potential, and it therefore allows for the calculation of all static thermodynamic properties, including vapor-liquid equilibrium data, by differentiation only. Phosgene is chosen as a candidate because of its industrial importance and the poor availability of corresponding laboratory measurement data in the literature due to its hazardous nature.

Introduction

There is a dire need for thermodynamic data in process engineering that cannot be satisfied by experimental measurements alone. Even though the available experimental database is in general increasing, it is obvious that traditional laboratory measurements are unable to keep up with the demand of industry. An empirical equation of state (EOS) correlation is an explicit relation between state variables and it can provide information for poorly investigated state points and properties by means of inter- and extrapolation schemes. The other advantage of an EOS is that it can summarize and represent tabulated data; even up to a level of accuracy where it can actually be used to calibrate experimental equipment. Such EOS are often referred to as reference quality EOS.¹ The construction of a reference quality EOS requires a large amount of experimental data, months or years of careful filtering of these data, and complex non-linear fitting. Consequently, there are less than ten substances privileged to have their own reference quality EOS correlations, such as water,² carbon dioxide,³ or nitrogen.⁴ For about 100 experimentally less studied substances, there are EOS correlations available that cover a considerably narrower range of states and may have a significantly lower accuracy than what is expected from a reference quality EOS.¹ Nonetheless, several equations from this category still offer a reasonable extrapolation behavior both in terms of states and thermodynamic properties for most process design purposes. For the remaining pure compounds of industrial relevance, there are typically insufficient data available to support highly accurate EOS development; and the data availability is much worse for mixtures. In any case, the most accurate and reliable EOS are regularly explicit empirical correlations of a thermodynamic potential.¹ This is intentional, since thermodynamic potentials play a special role in thermodynamics because they are different representations of the fundamental equation of state (FEOS) of thermodynamics and they carry the same information content. To be more specific, any other static thermodynamic property can be obtained from a combination of the partial derivatives of the thermodynamic potential with respect to its independent variables. These types of EOS are generally referred to as FEOS

correlations.

The problem of mapping the relevant fluid region of industrial interest with laboratory measurements is associated with high financial costs, the often extreme thermodynamic conditions, and the sometimes hazardous nature of the considered substance. The infamous chemical weapon of World War I, phosgene (CCl_2O , CAS: 75-44-5) is a good example. Being extremely toxic, with a fatal level of around 100 ppm over minutes of exposure,⁵ research institutions and laboratories unsurprisingly prefer to abstain from this substance, let alone systematically measure it. The available experimental data in the literature were measured 50 up to 100 years ago and essentially only consist of vapor-liquid equilibrium (VLE) data (saturated liquid density,⁶⁻¹⁰ vapor pressure,^{6,10-13} enthalpy of vaporization,^{10,13} and molar isobaric heat capacity of the saturated liquid^{9,10,13,14}), with the exception of the relatively recent measurements of the Wiltec Research Company that considered several state points in the homogenous region in addition to vapor pressure and saturated liquid density.¹⁵ Yet, the estimated world production of phosgene reached 1.3 million tons in 1977 and 2.7 million tons in 1996.⁵ The production rate has increased in the last twenty years because phosgene is used as an intermediate in numerous applications, including dye, pharmaceutical, agricultural, and mainly polymer industry, in presumably suboptimal processes due to insufficient thermophysical property data.

Molecular modeling and simulation has an advantage over experimental measurements that it is not limited by extreme conditions (temperature or pressure) or the nature of the substance. Moreover, it is associated with considerably lower financial cost and has typically a much faster response time. The predictive capability of molecular simulation is only dependent on the underlying molecular model that represents the targeted substance. It is generally accepted that atomistic molecular models can, and often do, provide reasonable thermodynamic properties for state points, properties, or scenarios that were not considered during the optimization of their parameters. Our previous findings with other substances showed that molecular models tend to perform reasonably well when comparing various

Helmholtz energy derivatives from simulations with the available FEOS correlations that are based on experimental data. The supplementary material of Ref.¹⁶ contains numerous examples. In fact, molecular models have evolved to a point when a seemingly notable disagreement between a single laboratory measurement and the corresponding result from molecular simulation does not immediately invalidate the latter. The strategy of using laboratory data along with molecular simulation results has recently been employed to develop FEOS for engineering purposes.¹⁷

The properties of phosgene render the substance an ideal candidate for molecular modelling and simulation and an effort of summarize and represent simulation data in the form of an FEOS. The purpose of this work is to investigate a simple fitting approach that is able to provide a reasonable FEOS correlation within extremely short notice and require essentially no expertise once an adequate molecular simulation data set is available. Today, such a data set can be generated within a few weeks on a couple of commodity computers.

Fundamental equation of state

Due to practical reasons, FEOS correlations are often explicit in terms of the thermodynamic potential

$$\alpha(\tau, \delta) = \frac{a^\circ(T, \rho) + a^r(T, \rho)}{RT} = \alpha^\circ(\tau, \delta) + \alpha^r(\tau, \delta), \quad (1)$$

with the molar Helmholtz energy a , the temperature T , the density ρ , the molar gas constant R , the inverse reduced temperature $\tau = T_c/T$, and the reduced density $\delta = \rho/\rho_c$, in which T_c is the critical temperature and ρ_c the critical density. The denominator renders α dimensionless. Eq. (1) shows that α can be additively separated into an ideal α° and a residual part α^r . The ideal part $\alpha^\circ(T, \rho) = \alpha^\circ(T) + \alpha^\circ(\rho)$ by definition corresponds to the value of $\alpha(T, \rho)$ when no intermolecular interactions are at work.¹ $\alpha^\circ(T, \rho)$ has a trivial density dependence $\alpha^\circ(\rho) = \ln(\rho/\rho_{\text{ref}})$ but a non-trivial temperature dependence. The latter is

often determined by spectroscopy or *ab initio* calculations. Although molecular models with internal degrees of freedom are parametrized to describe $\alpha^o(T)$ properly, the residual part $\alpha^r(T, \rho) = \alpha(T, \rho) - \alpha^o(T, \rho)$ is typically the target of molecular simulation. Accordingly, α^o and α^r are correlated separately during FEOS development with different mathematical functions.

For the present correlations, the ideal part was determined by integrating the isobaric heat capacity of the ideal gas state

$$\frac{c_p^o}{R} = 4 + \sum_{k=1}^3 v_k \frac{(u_k/T)^2 \exp(u_k/T)}{[\exp(u_k/T) - 1]^2}. \quad (2)$$

This equation was fitted to the data of Giauque and Ott¹⁴ for temperatures below 500 K and the data of Stull and Prophet¹⁸ for temperatures above 500 K (cf. Figure 1). The obtained parameters are $v_1 = 3.22652$, $v_2 = 1.23698$, $v_3 = 1.51143$, $u_1 = 874$ K, $u_2 = 2344$ K, and $u_3 = 445$ K. Because the c_p^o data from the literature are essentially derived from quantum statistical calculations and cannot be directly validated by experimental results, an uncertainty of $\pm 1\%$ can reasonably be assumed, although the literature data were reproduced here within $\pm 0.1\%$. In Figure 1, the deviation between the ideal part of the present FEOS and the correlation of DIPPR has a local minimum of -1.6% at 130 K. It is likely that the DIPPR correlation was not fitted to the corresponding literature c_p^o values since the data of Giauque and Ott¹⁴ are missing from the database at present.

The integration of Eq. (2) yields

$$\alpha^o(\tau) = \ln \delta + 3 \ln \tau + b_1 + b_2 \tau + \sum_{k=1}^3 v_k \ln [1 - \exp(-u_k \tau / T_c)], \quad (3)$$

where $b_1 = 8.3306265716$, $b_2 = -3.401313711$, while u_k and v_k are the same as those in Eq. (2). The integration constants b_1 and b_2 were specified such that the enthalpy $h = 0$ kJ·kg⁻¹ and the entropy $s = 0$ kJ·kg⁻¹·K⁻¹ at $T_0 = 298.15$ K and $p_0 = 1$ atm, and the corresponding ideal gas density is $\rho_0 = p_0 / (RT_0)$.

The empirical formula that represents $a^r/(RT)$ in this work consists of polynomial and exponential terms¹

$$\alpha^r(\tau, \delta) = \sum_{k=1}^{N_{\text{Pol}}} n_k \tau^{t_k} \delta^{d_k} + \sum_{k=N_{\text{Pol}}+1}^{N_{\text{Exp}}} n_k \tau^{t_k} \delta^{d_k} \exp(-\delta^{l_k}). \quad (4)$$

Additional types of terms, e.g. Gaussian bell-shaped or non-analytic,¹ were not considered here. The simultaneous optimization of the coefficients n_k , the exponents t_k , d_k , l_k , and the number and type of terms requires complex non-linear fit algorithms.^{1,19} Such an approach is vital for developing reference type FEOS, and it also requires a substantial amount of property data that goes through careful screening, which can easily take months or years and demands considerable expertise. Naturally, the optimization of industrial processes does not stay idle while FEOS are being developed. To provide a fast response time for industrial needs, the problem of insufficient data and long development time has to be tackled. An obvious solution to minimize the time requirement of FEOS fitting, is to use recommendations from the literature for the functional form of the correlation, as well as the values of the exponents t_k , d_k , l_k that were simultaneously optimized for a number of substances. There are a couple of such generalized parameter sets available: The 10- and the two 12-term FEOS from Span and Wagner (one 12-term FEOS is intended for polar and one 12-term FEOS for non- or weakly polar substances),^{1,20} or the 14-term FEOS from Sun and Ely are such correlations.²¹ In addition to these, the Bender²² (22-term) and the MBWR²³ (40-term) correlations were also tested here, using their functional form integrated to the Helmholtz energy representation according to Eq. (4).¹ With the present data set, the MBWR equation showed the best performance, and it is therefore presented in the following. Although the MBWR correlation has 40 terms, the parameter set of this correlation (cf. table 1), unlike generalized parameter sets, was originally optimized for a single substance (nitrogen) and the MBWR correlation in general is more likely to carry numerical instability or poor extrapolation behavior when applied to considerably different

substances. However, the need of extrapolation can be avoided, if a consistent data set containing a large number of thermodynamically non-redundant property information is sampled at systematically distributed state points covering the entire fluid range of interest. In contrast to laboratory work, molecular simulation renders such a data set feasible.

Fitting strategy and data set

The production of data sets by molecular simulation can be automatized and it is cheap. Furthermore, the formalism proposed by Lustig^{24,25} allows for the efficient generation of a large amount of thermodynamically non-redundant information. From a single molecular simulation run per state point, the method was designed to provide an arbitrary number of Helmholtz energy derivatives

$$A_{xy}^r = \tau^x \delta^y \frac{\partial^{x+y} \alpha^r(\tau, \delta)}{\partial \tau^x \partial \delta^y} = (1/T)^x \rho^y \frac{\partial^{x+y} \alpha^r(T, \rho)}{\partial (1/T)^x \partial \rho^y}, \quad (5)$$

with $x > 0$ or $y > 0$. These are exactly the derivatives of the thermodynamic potential in terms of which the FEOS is explicit, i.e. Eq. (1). Since α is a thermodynamic potential, any other static thermodynamic property is a combination of its partial derivatives. The molar internal energy u , pressure p , molar enthalpy h , molar Gibbs energy g , and molar isochoric heat capacity c_v are simple functions

$$\frac{u}{RT} = A_{10}^o(T) + A_{10}^r, \quad (6)$$

$$\frac{p}{\rho RT} = 1 + A_{01}^r, \quad (7)$$

$$\frac{1}{RT} \left(\frac{\partial p}{\partial \rho} \right)_T = 1 + 2A_{01}^r + A_{02}^r, \quad (8)$$

$$\frac{1}{\rho R} \left(\frac{\partial p}{\partial T} \right)_\rho = 1 + A_{01}^r - A_{11}^r, \quad (9)$$

$$\frac{h}{RT} = 1 + A_{01}^r + A_{10}^o(T) + A_{10}^r, \quad (10)$$

$$\frac{g}{RT} = 1 + A_{01}^r + A_{00}^o + A_{00}^r, \quad (11)$$

$$\frac{c_v}{R} = -A_{20}^o(T) - A_{20}^r, \quad (12)$$

while molar isobaric heat capacity c_p , and speed of sound w are non-linear combinations of derivatives

$$\frac{c_p}{R} = -A_{20}^o(T) - A_{20}^r + \frac{(1 + A_{01}^r - A_{11}^r)^2}{1 + 2A_{01}^r + A_{02}^r}, \quad (13)$$

$$\frac{Mw^2}{RT} = 1 + 2A_{01}^r + A_{02}^r - \frac{(1 + A_{01}^r - A_{11}^r)^2}{A_{20}^o(T) + A_{20}^r}, \quad (14)$$

where M is the molar mass, $A_{xy}^r = A_{xy}^r(T, \rho)$, and $A_{xy}^o = A_{xy}^o(T, \rho) = (1/T)^x \rho^y \cdot \partial^{x+y}[\alpha^o(T) + \alpha^o(\rho)]/\partial(1/T)^x/\partial\rho^y = A_{xy}^o(T) + A_{xy}^o(\rho)$. Note that the ideal part

- $A_{xy}^o(T, \rho) = 0$, for $x > 0$ and $y > 0$,
- $A_{xy}^o(T, \rho) = A_{xy}^o(T) + 0$, for $x > 0$ and $y = 0$,
- $A_{xy}^o(T, \rho) = 0 + (-1)^{1+y}$, for $x = 0$ and $y > 0$.

A more complete list of thermodynamic properties can be found in Ref.¹

Most of the derivatives A_{xy} cannot directly be measured in the laboratory. On the other hand, it is possible to produce a simulation data set that contains explicitly A_{xy} derivatives,

which is computationally convenient for FEOS correlation purposes: Each analytical derivative of Eq. (4) with respect to τ and δ provides an equation that is fitted to a result for A_{xy}^r from simulation. The total set of such equations needs to be solved only for the parameters n_k if the functional form and the exponents t_k , d_k , and l_k are specified (cf. Table 1). The number of equations is much larger than the number of variables n_k , thus the goal is to find an optimal set of n_k . This was done here with the algorithm for weighted multiproperty fits of Hust and McCarty.²⁶

In total, five derivatives, A_{10}^r , A_{01}^r , A_{20}^r , A_{11}^r , A_{02}^r , as well as A_{00}^r were sampled using the molecular simulation tool *ms2*²⁷ at 400 state points located in the homogeneous fluid region (cf. Figure 2) so that 2400 thermodynamically non-redundant records were generated. At each state point, 864 particles were equilibrated, and then sampled for two million production cycles with *NVT* ensemble Monte Carlo simulations²⁸ (number of particles N , volume V , and temperature T were held constant) using 16 processor cores per state point. The electrostatic long-range correction was treated by the reaction field method.²⁹ The simulations were based on the molecular model for phosgene of Huang et al.³⁰ that was optimized to vapor pressure, saturated liquid density, and heat of vaporization data from experiment between 270 K and 425 K. (The triple and critical point temperatures of phosgene are approximately 145 K and 455 K, respectively.). The model itself has no internal degrees of freedom and consists of four Lennard-Jones sites, a point dipole, and a point quadrupole. Details are given in the Appendix.

The statistical uncertainty of all simulation results was estimated with the method of Flyvbjerg and Petersen.³¹ Note that the statistical uncertainty of a molecular simulation result, by definition, cannot reflect any other factor than the inherent statistical nature of the simulation: At a given state point, M configurations on the molecular level are generated, and for each configuration thermodynamic properties are sampled. The final result for a thermodynamic property is the average of M values, and the statistical uncertainty of the result decreases as M increases.

A_{00}^r was determined by Widom’s test particle insertion³² by inserting 3456 test molecules in every production step. This method is associated with additional computational cost and has well known difficulties at high density, namely, it leads to A_{00}^r values with a large statistical uncertainty, both in absolute and relative terms. Because the statistical uncertainty of the simulation results serves as the weight of the fitted property during FEOS correlation,²⁶ data with high uncertainties practically do not influence the fit. Consequently, A_{00}^r results above $14 \text{ mol}\cdot\text{dm}^{-3}$ were discarded from the dense liquid region. The effect of removing every A_{00}^r data from the fitting procedure was also assessed, which is discussed below.

An obvious problem when generating such a data set is how to avoid sampling the solid and the two-phase regions. At first sight that seems to require some knowledge about the location of these regions. However, using the following procedure, no prior knowledge about the vapor-liquid equilibrium (VLE) or the solid-liquid equilibrium (SLE) is required:

1. Select two or three high temperature isotherms. Fit the FEOS to the simulation data along these isotherms and calculate a preliminary VLE envelope from it.
2. Remove state points if they are in the vapor-liquid two-phase region. Add more state points that are in the homogeneous fluid region.
3. Fit the FEOS to the extended set of state points, and calculate an updated VLE envelope. It is advised to keep a somewhat safe distance from the vapor-liquid two-phase region, because it is not guaranteed that the FEOS yields the VLE envelope that exactly corresponds to the molecular model.
4. Repeat steps (1) to (3) until the VLE envelope does not change significantly any more.

In case that a few state points accidentally remain in the vapor-liquid two-phase region, they likely do not significantly influence the overall fit quality if there is a sufficient number of other points sampled in the homogeneous fluid region. Nonetheless, the goal is to remove such state points. State points close to the solid state can be identified by monitoring the

mean square displacement of molecules from their initial positions. If the mean square displacement for the entire duration of the simulation is practically zero, then the state point is likely located very close to the solid state, and it should be removed.

Three iterations of this procedure are illustrated in Figure 2. Tests, considering other substances, indicate that the procedure requires about 3-6 iterations. For this iterative state point selection, the calculation of the VLE from the FEOS is essential and it is described in the Appendix.

Results and discussion

According to the database of the Design Institute for Physical Properties (DIPPR),³³ the critical temperature of phosgene is $T_c = 455 \text{ K} \pm 3\%$ and its critical density is $\rho_c = 5.25 \text{ mol}\cdot\text{dm}^{-3} \pm 10\%$ based on the currently available experimental data. The present FEOS correlation locates the critical point at $T_c = 462.88 \text{ K}$ and $\rho_c = 5.5916 \text{ mol}\cdot\text{dm}^{-3}$ using the method described in the appendix. The coefficients of the correlation fitted to the data at 400 state points from molecular simulation are listed in Table 1. The FEOS yields the critical pressure $p_c = 6.459 \text{ MPa}$; the corresponding value from DIPPR database is $p_c = 5.674 \pm 5\% \text{ MPa}$.

Statistical comparisons in the following are based on the relative and absolute deviation that are defined here for a given property X as

$$\text{RDEV}(X) = 100 \frac{(X_{\text{DATA}} - X_{\text{FEOS}})}{X_{\text{DATA}}}, \quad (15)$$

and

$$\text{ADEV}(X) = |X_{\text{DATA}} - X_{\text{FEOS}}|, \quad (16)$$

respectively.

Representation of data in the homogeneous region

There are very few laboratory data available in the literature concerning the homogeneous fluid region of phosgene. The Wiltec Research Company measured 20 p v T data points essentially along four isotherms.¹⁵ In those measurements, the phosgene sample was checked by gas chromatography and a single peak was detected. The sample itself was obtained after a single-stage distillation at 253.15 K from an initial sample that had a purity of > 99.0%. The temperature was measured with a platinum resistance thermometer calibrated to a NIST-traceable standard using the ITS-90 scale that had an accuracy of ± 0.05 K, while the pressure was measured with a Paroscientific pressure transducer having a NIST-traceable calibration that had an estimated accuracy of $\pm 0.03\%$. The density was estimated by first filling an initially evacuated cell (300 cm³) with phosgene at 273.15 K, and then removing phosgene increments and weighing them with a ± 0.002 g accuracy as the temperature or the pressure were gradually increased. The initial mass weighed to an accuracy of ± 0.02 g plus the removed phosgene content and the volume of the cell, which was determined through multiple calibrations with water as a function of temperature and pressure, yielded the density. The results of those measurements are listed in Table 2 along with the data from the present FEOS correlation. The relative deviations between the laboratory data (for pressure and density) and the present correlations increase in the vicinity of the critical point, but exceed $\pm 10\%$ only once.

In a considerably more complex FEOS development effort for ethylene oxide, in which molecular simulation data from the homogeneous region together with experimental VLE data were used and during which the coefficients and the exponents of an empirical FEOS correlation with polynomial, exponential, and Gaussian bell-shaped terms were optimized, the representation of A_{xy}^r results was found to be as follows for the majority of state points:¹⁷ A_{00}^r data were represented within $\pm 5\%$, A_{10}^r within $\pm 5\%$, A_{01}^r within $\pm 6\%$, A_{20}^r within $\pm 15\%$,

A_{11}^r within $\pm 5\%$, and A_{02}^r within $\pm 20\%$. According to Figure 3, the representation quality of the present FEOS is predominantly better. However, a direct comparison is not entirely fair, because the FEOS by Thol et. al.¹⁷ considered experimental as well as simulation data and even slight inconsistencies between the two may cause a deterioration in the representation of both. Nonetheless, with the present FEOS, the majority of state points are represented within $\pm 2\%$ for A_{00}^r , $\pm 1.5\%$ for A_{10}^r , $\pm 2\%$ for A_{01}^r , $\pm 8\%$ for A_{20}^r , $\pm 3\%$ for A_{11}^r , and $\pm 5\%$ for A_{02}^r , which is mostly within the statistical uncertainty of the simulation runs. Deviations with respect to potential simulation results close to the critical point may be higher than these percentages. Especially in case of A_{02}^r , it is important to note that simulation results at lower densities (below $4 \text{ mol}\cdot\text{dm}^{-3}$) are represented with seemingly large relative deviations. However, many of those data are in fact reproduced within their statistical uncertainty. Furthermore, at such low densities, large relative deviations are quite small in absolute terms. The absolute deviation plots in Figure 4 support this statement. The dimensionless absolute deviations shown there can be converted into SI units using Eqs. (1), (6), (7), (8), and (12): For A_{00}^r , A_{10}^r , and A_{02}^r , 0.001 in dimensionless units translates to $\approx 2 \text{ J}\cdot\text{mol}^{-1}$ at 250 K and $\approx 6 \text{ J}\cdot\text{mol}^{-1}$ at 750 K. For A_{01}^r , 0.01 in dimensionless units is $\approx 0.3 \text{ MPa}$ at 250 K and $16 \text{ mol}\cdot\text{dm}^{-3}$. For A_{20}^r , 0.1 in dimensionless units is $\approx 0.8 \text{ J}\cdot\text{mol}^{-1}\cdot\text{K}^{-1}$. The complete molecular simulation data set along with the corresponding values from the present FEOS is provided as supplementary material.

Finally, Figure 5 summarizes the performance of the FEOS in terms of usual thermodynamic properties. With only a few exceptions, properties were represented as follows: within $\pm 1.5\%$ for pressure, within $\pm 3\%$ for $(\partial p/\partial \rho)_T$, within $\pm 1.5\%$ for $(\partial p/\partial T)_\rho$, within $\pm 1.5\%$ for isochoric heat capacity, within $\pm 2\%$ for isobaric heat capacity, and within $\pm 1.5\%$ for speed of sound, which is mostly within the statistical uncertainty of the simulation runs. However, deviations seem to be consistently larger very close to the triple point (above $17 \text{ mol}\cdot\text{dm}^{-3}$ and below 175 K) for the isochoric and isobaric heat capacities, speed of sound, and $(\partial p/\partial T)_\rho$. Therefore, any information from the FEOS at this region should be treated with care.

Vapor-liquid equilibria and behavior of thermodynamic properties

VLE data from the present FEOS are predictions from homogeneous phase molecular simulation data and the subsequent fitting procedure. According to Figure 6, the present FEOS is fully consistent with the molecular model of phosgene as it predicts the VLE results from dedicated molecular simulation runs accurately.

The performance in comparison with the experimental data can also be seen in Figure 6. The saturated liquid density is represented within $\pm 2\%$. The vapor pressure plot between 300 K and the critical temperature shows acceptable deviations from laboratory measurements and their correlations. However, the deviation increases significantly below 300 K, although it should be mentioned that the model was practically not fitted to experimental data below 270 K because the uncertainty of VLE simulations increases with decreasing temperature. The large scatter of the vapor pressure simulation results can be clearly seen Figure 6 at low temperatures. Noticeably, there is a deviation between DIPPR and the most recent measurements by Jasperson et al.¹⁵ with respect to vapor pressure that increases gradually (0.2% at 260 K, 1.4% at 350 K, 5.0% at 440 K) approaching the critical temperature. According to Jasperson et al.,¹⁵ the deviation is due the almost seventy year old measurements upon which the DIPPR correlation is based involving outdated measurement methods, equipment, and the presumably low purity of the sample. Nonetheless, the pressure values at the critical point by Wiltec and DIPPR agree within the reported uncertainty of the latter ($\pm 5\%$). Enthalpy of vaporization data, which are questionable in general, are represented with -4% and up to -8% deviation by the present FEOS. Literature data for the isobaric heat capacity of the saturated liquid are available between 145 K and 280 K, which is essentially out of the temperature range of the present model. Nonetheless, the experimental values are represented with around $+10\%$ deviation. In light of the general trends shown in Figure 6, it is advised to use the available correlations^{15,33} instead of the present FEOS to obtain the VLE data of phosgene.

Figure 7 shows the general physical behavior of the most important thermodynamic proper-

ties. The qualitative behavior of the thermodynamic properties is well-known.¹⁹ In the T vs. ρ diagram (Figure 7, top left) the rectilinear diameter is usually almost a straight line up to the vicinity of the critical point where it may show a slight curvature. Here, the algorithm employed to locate the critical density yields a value that causes a pronounced bend in the rectilinear diameter approaching the critical temperature. We are unable to provide further comments whether this bend is an artifact of the algorithm or it is really consistent with the molecular model. However, a similar behavior has been observed in a previous work, other earlier mentioned generalized FEOS that were fitted to a simulation based data set.³⁴

In the p vs. ρ plot (Figure 7, top right), the isotherms should converge, but not cross each other at high temperature, pressure, or density. For the residual isochoric heat capacity c_v^r (Figure 7, mid left), the saturated liquid line should have a curvature and rise towards low temperatures. In accordance with the speed of sound minimum at the critical point (Figure 7, mid right), the residual isochoric heat capacity should have a maximum there. Furthermore, the speed of sound should have a negative slope and no curvature at low temperatures in the liquid phase. The second virial coefficient B (Figure 7, bottom left) should be negative for low temperatures, cross the zero line once, and then approach zero after passing through a maximum. B can be calculated for molecular models up arbitrary accuracy with simple numerical integration schemes.³⁵ The corresponding results agree well with the present FEOS. The characteristic curves (Figure 7, bottom right) should be smooth with no unusual curvature within the limits of the data set.

Interpolation performance: Effect of data set reduction

To apply the workflow presented here in practice, the computational bottleneck is carrying out 400 molecular simulation runs with 3456 test molecule insertions in every production step to calculate A_{00}^r . To test if such an effort is really necessary, a considerably smaller data set was created by keeping every third state point (133 in total) along the isotherms of the original one with 400 state points shown on Figure 2. After performing a new fit with the

133 state points and excluding A_{00}^r entirely from the fit, it was concluded that this serious reduction barely affected the overall performance: The derivatives, including A_{00}^r , calculated at the original 400 state points were represented with practically the same quality as before. The corresponding figures, that are analogous to Figures 3, 4, and 5, showing the effect of the reduction of the data set, are provided as supplementary material. The performance with respect to VLE data and the experimental homogeneous data (Figure 6 and Table 2) remained practically identical after the reduction.

The low importance of A_{00}^r values in the data set is not surprising. Its derivatives describe the Helmholtz energy surface much more accurately than A_{00}^r itself when sampling about 400 state points. Furthermore, A_{10}^r (energy) and A_{01}^r (pressure) are the most well-behaved properties from molecular simulation and fitting them with a high accuracy essentially guarantees a perfect match for A_{00}^r as well. These findings indicate that a similarly valuable data set can be created even on a couple of commodity computers within a few days and without considerable performance loss.

Conclusion

In this work, an empirical FEOS correlation was fitted to molecular simulation data and serves predictive purposes. The underlying data set contains six properties at 400 state points resulting in a set of 2400 thermodynamically non-redundant data points. These thermodynamic properties along with the available experimental pressure and density data in the homogeneous fluid region are represented well by the present FEOS. Furthermore, an almost identical performance was achieved when the fitting procedure was repeated with a considerably smaller and computationally less costly data set. Moreover, the VLE results of dedicated molecular simulations were predicted accurately from the underlying homogeneous data and the subsequent FEOS fitting. The VLE data from experimental measurements can still be more accurately reproduced with existing experimental VLE only correlations^{15,33}

than with the molecular model of phosgene. The FEOS correlation of this work is provided as supplementary material.

The workflow presented here was devised such that it requires very little human interaction and almost no expertise while offering a fast response time. It was implemented into a cloud computing environment that offers a web-based user interface to select state points and the underlying molecular model. Simulation runs and FEOS fitting are carried out automatically on dedicated high performance computers, and thus the effort requires no computational resources from the user. Details will be published shortly.

Acknowledgments

The authors gratefully acknowledge financial support by Deutsche Forschungsgemeinschaft under the grant VR6/4-1. This work was carried out under the auspices of the Boltzmann-Zuse Society (BZS) of Computational Molecular Engineering. Access to hardware was given by the High Performance Computing Center Stuttgart (HLRS) under grant MMHBF2. The authors also would like to thank Monika Thol for her support in preparing figures and setting up the ideal part of the FEOS, as well as Louis V. Jasperson for providing laboratory measurement data in an electronic form.

Supporting Information Available

The supplementary material contains the complete underlying data set from molecular simulation along with the corresponding values from the present FEOS (including VLE data) that can be used to verify computer implementation. The present FEOS is provided as C++ code and an FLD file. The latter serves as input file for the software REFPROP³⁶ distributed by the National Institute of Standards and Technology. Additional figures are also included that show the effect of data set reduction.

This material is available free of charge via the Internet at <http://pubs.acs.org/>.

Molecular model

The coordinates and parameters for the molecular model of phosgene are given in Table 3.

Vapor-liquid equilibrium calculation

For locating the vapor pressure and the corresponding saturated vapor and saturated liquid densities, an algorithm was chosen that is based on the method of Szalai et al.³⁷ Expanding the chemical potential μ and the pressure p in a Taylor series around a known state point (p_0, ρ_0) yields

$$\mu = \mu_0 + \left(\frac{\partial \mu}{\partial p} \right)_T (p - p_0) + \dots, \quad (17)$$

and

$$p = p_0 + \left(\frac{\partial p}{\partial \rho} \right)_T (\rho - \rho_0) + \dots. \quad (18)$$

Keeping the linear terms, using the relation $(\partial \mu / \partial p)_T = (\partial g / \partial p)_T = V/N = 1/\rho$, that holds for pure fluids, and applying the phase equilibrium conditions $\mu^L = \mu^V$ and $p^L = p^V = p_v$ at a given temperature leads to

$$\mu_0^L + \frac{1}{\rho_0^L} (p_v - p_0^L) = \mu_0^V + \frac{1}{\rho_0^V} (p_v - p_0^V), \quad (19)$$

and

$$p_0^L + \left(\frac{\partial p}{\partial \rho} \right)_T^L (\rho^L - \rho_0^L) = p_0^V + \left(\frac{\partial p}{\partial \rho} \right)_T^V (\rho^V - \rho_0^V) = p_v. \quad (20)$$

Eq. (19) yields the vapor pressure p_v

$$p_v = \frac{(\mu_0^L - p_0^L/\rho_0^L) - (\mu_0^V - p_0^V/\rho_0^V)}{1/\rho_0^V - 1/\rho_0^L}, \quad (21)$$

and Eq. (20) provides the saturated densities ρ^L and ρ^V

$$\rho^{L,V} = \frac{p_v - p_0^{L,V}}{(\partial p/\partial \rho)_T^{L,V}} + \rho_0^{L,V}, \quad (22)$$

where the superscripts L and V stand for liquid and vapor, respectively. Note that the variables in Eqs. (21) and (22), i.e. p_0 , μ_0 , and $(\partial p/\partial \rho)_T$ at state point (T, ρ_0) , that are required to calculate p_v and $\rho^{L,V}$ are directly obtainable from the residual part of the FEOS correlation (including μ_0 , because the exclusively temperature dependent ideal part of the total chemical potential cancels out in Eq. (19)). Naturally, increasing the number of terms considered in the Taylor series up to arbitrary order would yield the vapor pressure and the coexisting densities at a given temperature immediately. However, this might be an unrealistic expectation towards the FEOS correlation, because it would have to provide precise values for the required derivatives $(\partial^2 \mu/\partial p^2)_T$, $(\partial^3 \mu/\partial p^3)_T$, ..., $(\partial^2 p/\partial \rho^2)_T$, $(\partial^3 p/\partial \rho^3)_T$, It is more suitable to find the VLE in finite steps applying Eq. (22) successively in an iterative manner: At a given temperature T and densities $\rho_j^{L,V}$, $p_j^{L,V}$, $\mu_j^{L,V}$, and $(\partial p/\partial \rho)_T^{L,V}$ are calculated for step j . Substituting these values into Eq. (21) provides the vapor pressure p_v for step j , and since p_v is known, Eq. (22) yields ρ_{j+1}^L and ρ_{j+1}^V for step $j+1$. Starting with some initial $\rho_0^{L,V}$, that must be in the homogeneous phase, the iterative process continues until the criteria $\mu_j^L - \mu_j^V < d$ and $p_j^L - p_j^V < d$ are satisfied for an arbitrarily small d . Upon convergence, the saturated densities $\rho_j^{L,V} = \rho^{L,V}$ and the vapor pressure $p_j^L = p_j^V = p_v$ at a given temperature are known. The VLE envelope itself can be obtained by locating the saturated densities for a series of temperature values starting at $T_{min} < T_c$. Eq. (22) ceases to yield distinct coexisting densities if the critical temperature is exceeded. Consequently, T_c and ρ_c can be determined up to an arbitrary numerical accuracy.

It has to be noted that when fitting Eq. (4) and just simply using some arbitrary values for T_c and ρ_c in Eq. (4), the FEOS itself is unlikely to identify the very same values as the actual critical temperature and critical density of the FEOS for which $[\partial p(T_c, \rho_c)/\partial \rho]_T = [\partial^2 p(T_c, \rho_c)/\partial \rho^2]_T = 0$. In case these conditions are constrained at T_c and ρ_c , the FEOS yields the critical point at T_c and ρ_c . If they are not constrained, the actual critical temperature and density of the FEOS can still be determined by a simple iterative approach. One iteration step consists of the following three substeps:

1. Perform the FEOS fit using T_c^i and ρ_c^i in Eq. (4).
2. Determine the actual critical temperature T_c' and density ρ_c' of this fit.
3. Update the critical temperature and density used in Eq. (4) according to $T_c^{i+1} = \lambda T_c' + (1 - \lambda)T_c^i$ and $\rho_c^{i+1} = \lambda \rho_c' + (1 - \lambda)\rho_c^i$, where $0 \leq \lambda \leq 1$ with typical values between 0.1 and 0.5.

These substeps should be repeated until the critical temperature and density converge to finite values, although it should be mentioned that convergence is not guaranteed. However, a very rough guess for the initial values of T_c and ρ_c is perfectly satisfactory.

References

- (1) Span, R. *Multiparameter Equations of State: An Accurate Source of Thermodynamic Property Data*; Springer Verlag, Berlin, 2000.
- (2) Wagner, W.; Pruss, A. *J. Phys. Chem. Ref. Data* **2002**, *31*, 387–535.
- (3) Span, R.; Wagner, W. *J. Phys. Chem. Ref. Data* **1996**, *25*, 1509–1596.
- (4) Span, R.; Lemmon, E. W.; Jacobsen, R. T.; Wagner, W.; Yokozeki, A. *J. Phys. Chem. Ref. Data* **2000**, *29*, 1361–1433.

- (5) Ryan, T.; Seddon, E.; Seddon, K.; Ryan, C. *Phosgene: and Related Carbonyl Halides*; Topics in Inorganic and General Chemistry; Elsevier Science, Amsterdam, 1996.
- (6) Paterno, E.; Mazzucchelli, A. *Gazz. Chim. Ital.* **1920**, *50*, 30–53.
- (7) Germann, A. F. O. *J. Phys. Chem.* **1925**, *29*, 138–141.
- (8) Davies, C. N. *J. Chem. Phys.* **1946**, *14*, 48–49.
- (9) Timmermans, J. *Physico-Chemical Constants of Pure Organic Compounds, Vol II*; Elsevier, New York, NY, 1965.
- (10) Braker, W.; Mossman, A. L. *Matheson Unabridged Gas Data Book: A Compilation of Physical and Thermodynamic Properties of Gases*; Matheson Company, New Jersey, NJ, 1974.
- (11) Germann, A. F. O.; Taylor, Q. W. *J. Am. Chem. Soc.* **1926**, *48*, 1154–1159.
- (12) Stull, D. R. *Ind. Eng. Chem.* **1947**, *39*, 517–540.
- (13) Giaque, W. F.; Jones, W. M. *J. Am. Chem. Soc.* **1948**, *70*, 120–124.
- (14) Giaque, W. F.; Ott, J. B. *J. Am. Chem. Soc.* **1960**, *82*, 2689–2695.
- (15) Jaspersen, L. V.; Wilson, G. M.; Wilson, L. C. *Vapor Pressures, Critical Properties, and High Pressure PVT Measurements on Phosgene*; AIChE Spring Meeting, 1996.
- (16) Rutkai, G.; Thol, M.; Lustig, R.; Span, R.; Vrabec, J. *J. Chem. Phys.* **2013**, *139*, 041102.
- (17) Thol, M.; Rutkai, G.; Koster, A.; Kortmann, M.; Span, R.; Vrabec, J. *Chem. Eng. Sci.* **2015**, *121*, 87–99.
- (18) Stull, D. R.; Prophet, H. *JANAF Thermochemical Tables, 2nd ed., NSRDS-NBS 37*; U.S. Department of Commerce, Washington, D.C., 1971.

- (19) Lemmon, E. W.; Jacobsen, R. T. *J. Phys. Chem. Ref. Data* **2005**, *34*, 69–108.
- (20) Span, R.; Wagner, W. *Int. J. Thermophys.* **2003**, *24*, 1–39.
- (21) Sun, L.; Ely, J. F. *Int. J. Thermophys.* **2005**, *26*, 705–728.
- (22) Bender, E. Equations of state exactly representing the phase behavior of pure substances. Proceedings of the Fifth Symposium on Thermophys. Prop., ASME, New York. 1970.
- (23) Jacobsen, R. T.; Stewart, R. B. *J. Phys. Chem. Ref. Data* **1973**, *2*, 757–922.
- (24) Lustig, R. *Mol. Sim.* **2011**, *37*, 457–465.
- (25) Lustig, R. *Mol. Phys.* **2012**, *110*, 3041–3052.
- (26) Hust, J.; McCarty, R. *Cryogenics* **1967**, *7*, 200–206.
- (27) Glass, C. W.; Reiser, S.; Rutkai, G.; Deublein, S.; Koster, A.; Guevara-Carrion, G.; Wafai, A.; Horsch, M.; Bernreuther, M.; Windmann, T.; Hasse, H.; Vrabec, J. *Comput. Phys. Commun.* **2014**, *185*, 3302–3306.
- (28) Frenkel, D.; Smit, B. *Understanding Molecular Simulation: From Algorithms to Applications*; Academic Press, Elsevier, San Diego, CA, 2002.
- (29) Barker, J. A.; Watts, R. O. *Mol. Phys.* **1973**, *26*, 789–792.
- (30) Huang, Y.-L.; Heilig, M.; Hasse, H.; Vrabec, J. *AIChE J.* **2011**, *57*, 1043–1060.
- (31) Flyvbjerg, H.; Petersen, H. G. *J. Chem. Phys.* **1989**, *91*, 461–466.
- (32) Widom, B. *J. Chem. Phys.* **1963**, *39*, 2808–2812.
- (33) Rowley, R. L.; Wilding, W. V.; Oscarson, J. L.; Yang, Y.; ; Zundel, N. A.; Daubert, T. E.; Danner, R. P. *DIPPR Data Compilation of Pure Compound Properties: Design Institute for Physical Properties*; AIChE, New York, NY, 2006.

- (34) Lustig, R.; Rutkai, G.; Vrabec, J. *Mol. Phys.* **2015**, *113*, 910–931.
- (35) Hirschfelder, J. O.; Curtiss, C. F.; Bird, R. B.; Mayer, M. G. *Molecular theory of gases and liquids*; Wiley New York, 1954; Vol. 26.
- (36) NIST Reference Fluid Thermodynamic and Transport Properties Database.
<http://www.nist.gov/srd/nist23.cfm>.
- (37) Szalai, I.; Liszi, J.; Boda, D. *Chem. Phys. Lett.* **1995**, *246*, 214–220.
- (38) Vrabec, J.; Hasse, H. *Mol. Phys.* **2002**, *100*, 3375–3383.
- (39) Vrabec, J.; Kettler, M.; Hasse, H. *Chem. Phys. Lett.* **2002**, *356*, 431–436.

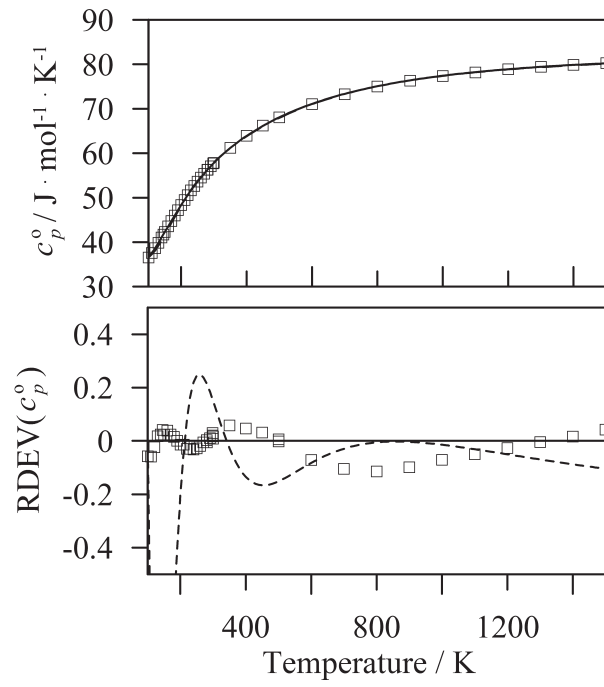


Figure 1: Isobaric heat capacity of the ideal gas state c_p^0 : - - correlation of DIPPR;³³ — present FEOS; \square data from the literature^{14,18} (top). Relative deviations (RDEV) were calculated by Eq. (15) (bottom).

Table 1: Parameters of Eq. (4). The exponents t_k , d_k , and l_k were taken from the MBWR correlation.²³ The coefficients n_k were determined in the present work.

k	t_k	d_k	l_k	n_k
1	0	1		-0.095842094249538
2	0.5	1		3.060952615139520
3	1	1		-4.747603241620660
4	2	1		1.338877244191170
5	3	1		-0.703848906445479
6	0	2		0.130746087315180
7	1	2		-0.185421337994230
8	2	2		0.323226318151166
9	3	2		0.390419782002820
10	0	3		0.029302442911150
11	1	3		-0.042207175336127
12	2	3		-0.079579086717665
13	1	4		0.068455977731017
14	2	5		-0.065766198173309
15	3	5		0.014775785350582
16	2	6		0.020058202738120
17	2	7		-0.001302560740835
18	3	7		-0.002862077171645
19	3	8		0.000471671584767
20	3	0		-1.992569767335400
21	4	0		-0.072342927646866
22	5	0		0.004522322999102
23	3	0	2	1.992557973563120
24	4	0	2	0.072428420215191
25	5	0	2	-0.004564386771021
26	3	2	2	1.311876945126580
27	4	2	2	0.659818243382377
28	5	2	2	-0.343829613759978
29	3	4	2	0.560294166439144
30	4	4	2	0.096613261111098
31	5	4	2	0.048621442800266
32	3	6	2	-0.009280163441566
33	4	6	2	0.137750035189476
34	5	6	2	0.018998019880235
35	3	8	2	0.042226707042714
36	4	8	2	0.007823270710127
37	5	8	2	-0.023062729469879
38	3	10	2	-0.008317628227420
39	4	10	2	0.011568386045278
40	5	10	2	0.001358217519838

Table 2: Comparison of experimental $p\nu T$ data¹⁵ (EXP) from the homogeneous fluid region with the present correlation (FEOS). Comparisons are also expressed in terms of relative deviations (RDEV) calculated by Eq. (15). The third column lists the density from the present FEOS at the temperature and pressure specified by the laboratory $p\nu T$ data, while the sixth column is the pressure from the present FEOS at the temperature and density specified by the laboratory $p\nu T$ data.

T/K	$\rho/\text{mol}\cdot\text{dm}^{-3}$		RDEV(ρ)	p/MPa		RDEV(p)
	EXP	FEOS		EXP	FEOS	
423.153	10.942	10.870	0.7	13.631	14.678	-7.7
423.150	10.674	10.618	0.5	10.397	11.054	-6.3
423.157	10.300	10.273	0.3	6.909	7.140	-3.3
423.161	9.876	9.898	-0.2	4.158	4.023	3.2
443.149	10.290	10.191	1.0	13.776	14.831	-7.7
443.144	9.884	9.806	0.8	10.335	10.947	-5.9
443.151	9.254	9.228	0.3	6.895	7.013	-1.7
443.156	8.819	8.855	-0.4	5.509	5.400	2.0
473.148	8.975	8.828	1.6	13.003	13.821	-6.3
473.176	8.307	8.171	1.6	10.328	10.770	-4.3
473.200	5.926	5.082	14.2	7.329	7.562	-3.2
473.200	2.551	2.347	8.0	5.688	5.922	-4.1
473.150	1.180	1.129	4.3	3.537	3.659	-3.4
498.136	7.938	7.729	2.6	13.817	14.587	-5.6
498.143	6.375	6.023	5.5	10.370	10.809	-4.2
498.132	4.472	4.033	9.8	8.522	8.924	-4.7
498.134	2.933	2.727	7.0	7.026	7.307	-4.0
498.134	2.058	1.954	5.1	5.743	5.942	-3.5
498.134	1.450	1.380	4.8	4.488	4.657	-3.8
498.134	1.024	0.982	4.1	3.427	3.547	-3.5

Table 3: Sigma (σ) and epsilon (ϵ) denote the length and energy parameter of the Lennard-Jones (LJ) potential, respectively. k_B is the Boltzmann constant. D denotes the dipole moment of the point dipole and Q the quadrupole moment of the point quadrupole. All coordinates are in principal axes with respect to the center of mass. The orientation of the point dipole is defined with Euler angles: φ is the azimuthal angle with respect to the x - y -plane and θ is the inclination angle with respect to the z -axis.

Site	$x/\text{\AA}$	$y/\text{\AA}$	$z/\text{\AA}$	$\sigma/\text{\AA}$	$\epsilon \cdot k_B^{-1}/\text{K}$	θ/deg	φ/deg	$D/\text{Cm} \cdot 10^{-30}$	$Q/\text{Cm}^2 \cdot 10^{-40}$
C	0	0.5049	0	2.815	10.62				
O	0	1.7018	0	3.195	132.66				
Cl	0	-0.4695	-1.4509	3.366	157.63				
Cl	0	-0.4695	1.4509	3.366	157.63				
Dipole	0	0.0845	0			90	90	3.341	
Quadrupole	0	0	0			90	90		-12.098

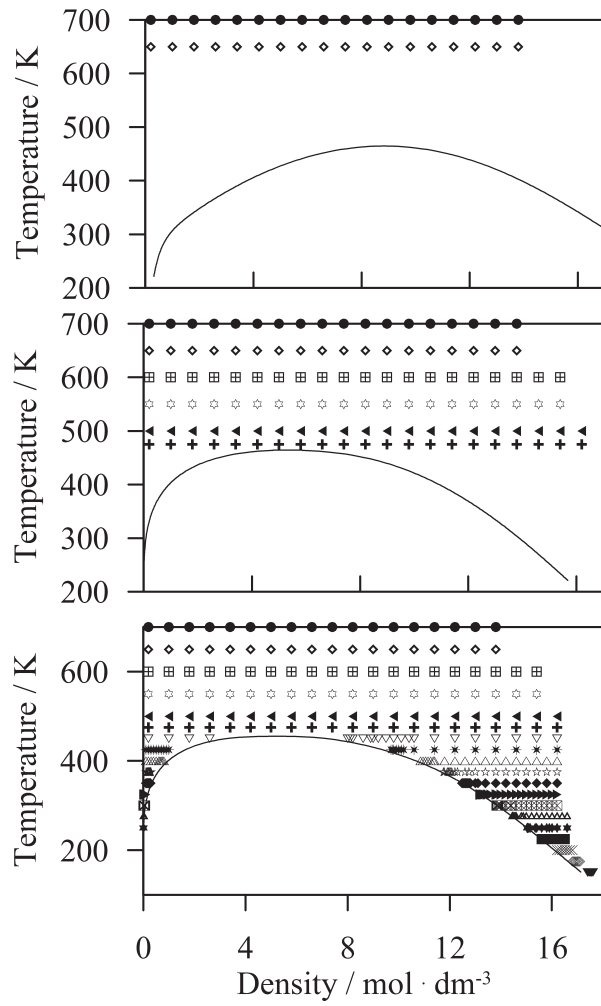


Figure 2: State points located in the homogeneous fluid region were selected in three consecutive steps according to the method described in this section. After the third iteration, the present data set contained 400 state points. The continuous curve delimits the vapor-liquid two-phase region calculated at the current iteration.

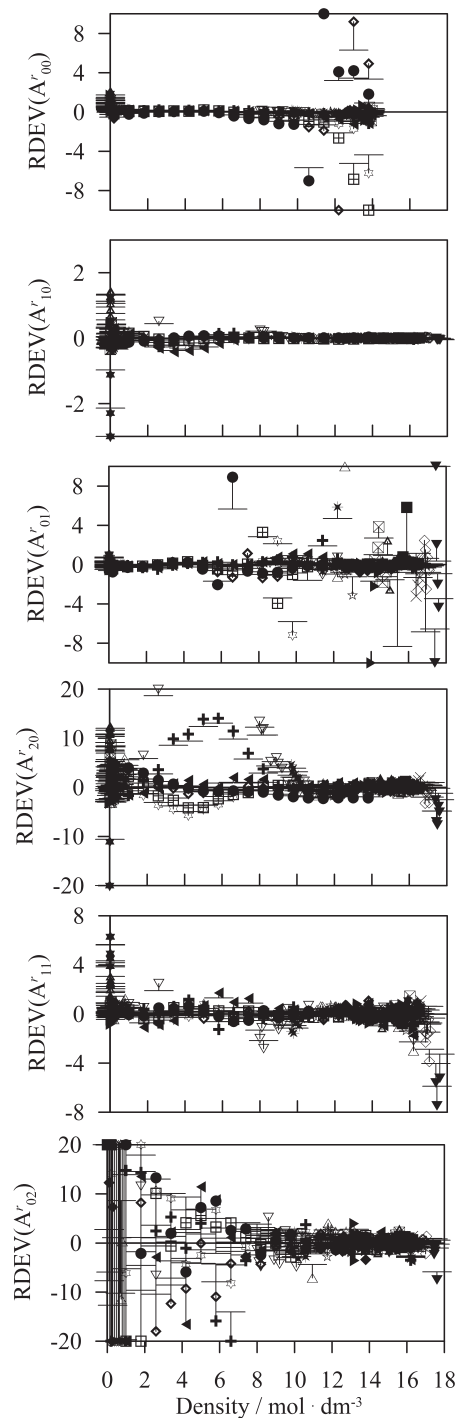


Figure 3: Relative deviations (RDEV) calculated by Eq. (15) between molecular simulation data of this work and the present FEOS. The comparisons include the entire data set of 400 state points from the homogeneous fluid region shown in Figure 2. Different symbols denote different isotherms and the notation corresponds to the one in Figure 2. RDEV values that exceeded the vertical axis limits were placed on the borders of the axis, but the spread of error bars of these points reflects the uncertainty with respect to their original locations. Error bars are plotted only in one direction for better visibility.

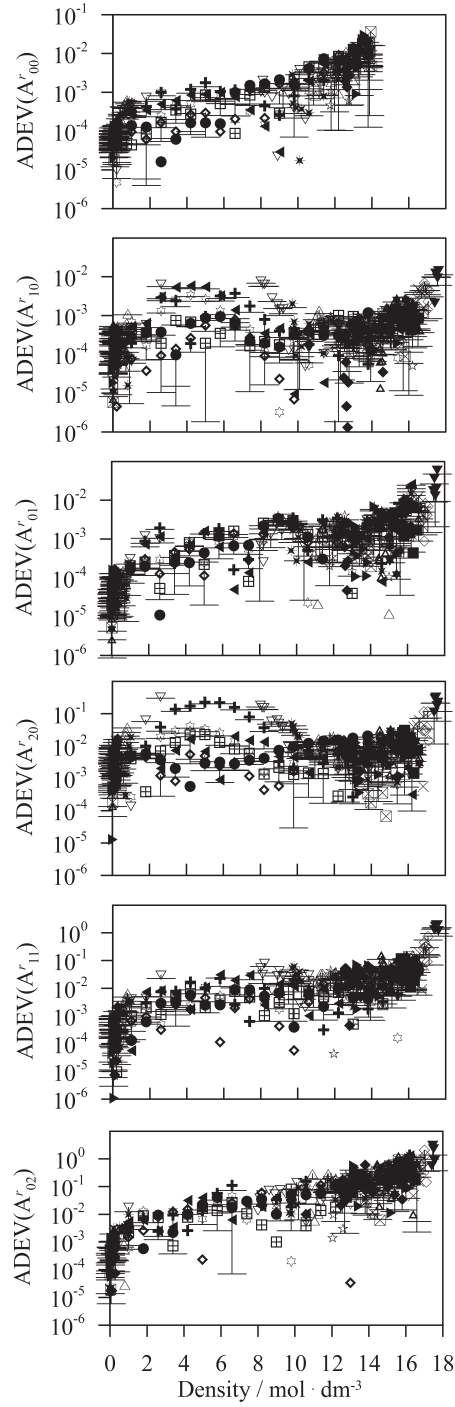


Figure 4: Absolute deviations (ADEV) calculated by Eq. (16) between molecular simulation data of this work and the present FEOS. Details are as in Figure 3.

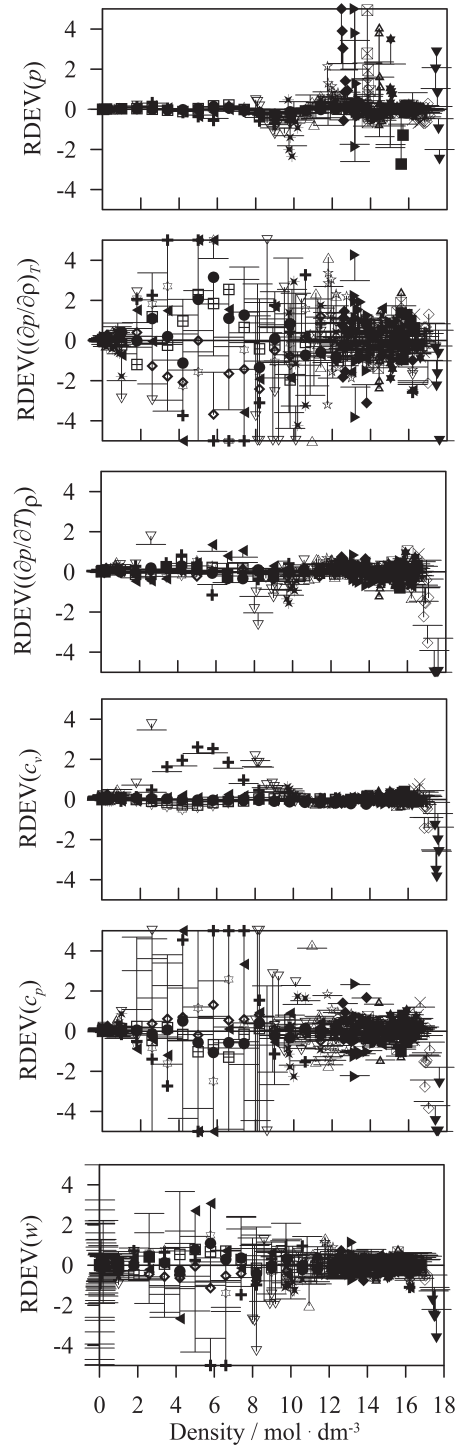


Figure 5: Relative deviations (RDEV) calculated by Eq. (15) between molecular simulation data of this work and the present FEOS. Details are as in Figure 3.

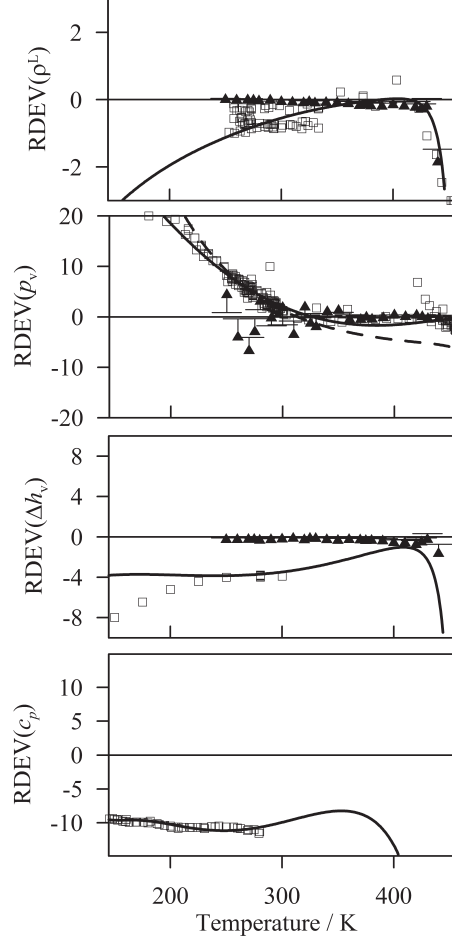


Figure 6: Relative deviations according to Eq. (15) between the present FEOS and data from the literature: \square experimental data (saturated liquid density ρ^L ,⁶⁻¹⁰ vapor pressure p_v ,^{6,10-13} enthalpy of vaporization Δh_v ,^{10,13} and molar isobaric heat capacity c_p ^{9,10,13,14}); \blacktriangle dedicated VLE simulations of this work using the molecular simulation tool *ms2*²⁷ with the grand equilibrium method,³⁸ 864 particles in the liquid phase, around 500 particles in the vapor phase, and with the gradual insertion technique³⁹ applied instead of Widom's method³² to calculate the chemical potential below 300 K; — correlation of DIPPR;³³ - - correlation of Jasperson et al.¹⁵ The vapor pressure correlation of Jasperson et al. is exclusively based on their own laboratory measurements and represents those data with very high accuracy: $\pm 0.04\%$ on average, where the representation of an individual value never exceeds $\pm 0.17\%$. Error bars are plotted only in one direction for better visibility.

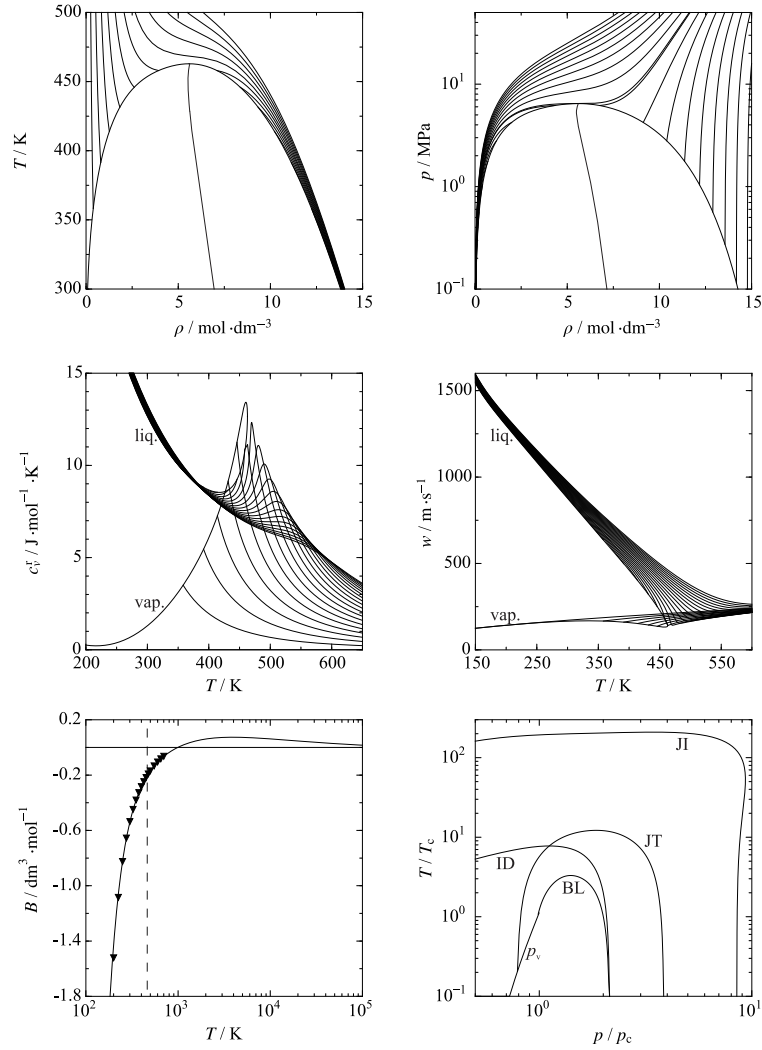


Figure 7: Physical behavior of the thermodynamic properties p , w , c_v^r , B (second virial coefficient) as well as characteristic curves: JI - Joule inversion curve ($A_{11}^r = 0$); JTI - Joule-Thomson inversion curve ($A_{01}^r + A_{02}^r + A_{11}^r = 0$); ID - ideal curve ($A_{01}^r = 0$); BL - Boyle curve ($A_{01}^r + A_{02}^r = 0$); p_v - vapor pressure. \blacktriangledown dedicated second virial coefficient calculations of this work; - - the critical temperature.